

# Dynamics of azimuthal thermoacoustic modes in imperfectly symmetric annular geometries

Thomas Indlekofer,<sup>1,\*</sup> Abel Faure-Beaulieu,<sup>2</sup> James R. Dawson,<sup>1</sup> and Nicolas Noiray<sup>2,†</sup>

<sup>1</sup>*Department of Energy and Process Engineering,  
Norwegian University of Science and Technology, Trondheim, Norway*

<sup>2</sup>*CAPS Laboratory, Department of Mechanical and Process Engineering, ETH Zürich  
(Dated: April 16, 2021)*

Using a nominally symmetric annular combustor, we present experimental evidence of a predicted spontaneous symmetry breaking and an unexpected explicit symmetry breaking in the neighborhood of the Hopf bifurcation, which separates linearly-stable azimuthal thermoacoustic modes from self-oscillating modes. We derive and solve a multidimensional Fokker-Planck equation to unravel a unified picture of the phase space topology. We demonstrate that symmetric probability density functions of the thermoacoustic state vector are elusive, because the effect of asymmetries, even imperceptible ones, is magnified close to the bifurcation.

Symmetry breaking in systems where waves propagate along closed loops or spheres occur in a wide variety of physical problems. Examples range from Bose-Einstein condensates in toroidal traps [1, 2], whispering gallery modes in optomechanical resonators [3–5], counter-propagating modes in optical ring cavities [6], nonreciprocal acoustic circulators [7], intrinsic rotation in Tokamak plasmas [8], to sporadic reversal in direction of planetary dynamo waves [9, 10]. Symmetry breaking is also ubiquitous in fluid mechanics [11], for example in von-Kármán swirling flows with counter-rotating toroidal vortices [12–14]. Recently, symmetry breaking was observed for azimuthal thermoacoustic modes in annular combustors typically found in jet engines or power generation gas turbines. First described by Lord Rayleigh [15], thermoacoustic instabilities that arise from a constructive coupling between the acoustic field and the heat release rate of the flames lead to damaging vibrations. Azimuthal thermoacoustic modes have been investigated in real engines [16–18], laboratory experiments [19–21] and numerical simulations [22]. Over the last decade, the dynamic nature of these modes has received significant attention [23], and the following classification has been established: standing modes, whose nodal line direction remains constant or slowly drifts around the annular chamber, spinning modes, whose nodal line spins at the speed of sound, or a combination of both referred to as mixed modes can exist. Several studies focused on the effects of clearly identified combustor asymmetries, e.g. [24–28], and several reduced-order models [29–38] were proposed to explain experimental observations with limited success. Notably, a recently proposed ansatz for describing the acoustic field [39] was combined with the wave equation to describe an ideal annular combustor, unifying previous theoretical frameworks [40]. However, the transition from linearly stable to self-oscillating azimuthal thermoacoustic modes has never been investigated. In this letter, we fill this gap with experimental data showing that the route to a self-sustained quasi-pure

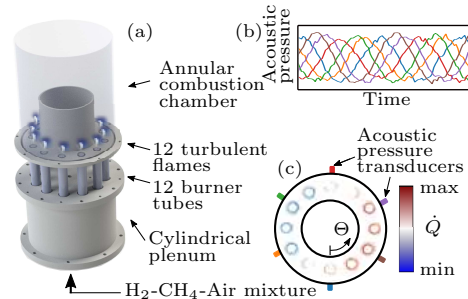


FIG. 1. (a) Model gas turbine combustor. (b) Acoustic pressure recorded with 6 transducers. During the selected interval, the thermoacoustic limit-cycle is a quasi-purely spinning eigenmode. (c) Phase-averaged flame chemiluminescence.

spinning mode passes through stationary states that are characterized by a statistically prevailing standing mode and intermittent reversals of spinning direction. We also build upon the model from [40] to unravel the complex topology of the phase space to demonstrate that symmetrically designed combustors will always display explicit symmetry breaking of the thermoacoustic modes at the bifurcation.

*Experimental evidence of explicit and spontaneous symmetry breaking.*—Experiments were conducted using an annular combustor with 12 premixed flames operated at atmospheric condition (see Fig. 1) and fueled with a mixture of 70%  $H_2$  and 30%  $CH_4$  by power. The thermal power was fixed to 72 kW and the equivalence ratio was varied between 0.4875 and 0.575. Twelve pressure transducers were mounted at six azimuthal positions flush with the inner wall of the burner tubes [41] and recorded with a sampling rate of 51.2 kHz. The natural chemiluminescence of the flames viewed from the exhaust is recorded with a high speed camera using the same optical system as in [24]. For each  $\Phi$ , the combustor was ignited, run for at least 60 s to reach thermal equilibrium before recording 100 s of acoustic data while keeping the operating condition constant, and then turned off. The sound pressure level (SPL) in the annular combustor is

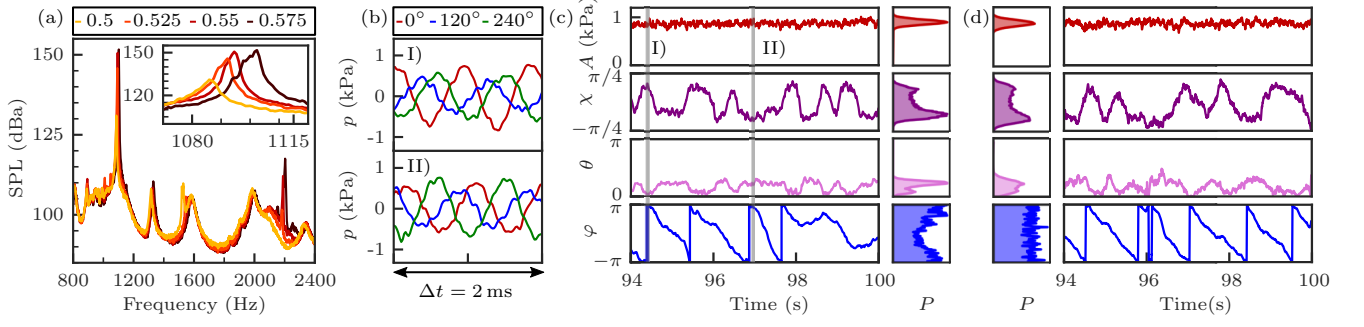


FIG. 2. (a) SPL for increasing  $\Phi$ . (b) Selected intervals for  $\Phi = 0.55$ , during which the azimuthal mode is mixed, with CW and CCW spinning directions. The angles in the legend correspond to the locations of the transducers. (c) Evolution of slow-flow variables that define the state of the azimuthal thermoacoustic mode, during the last 6 seconds of the record for  $\Phi = 0.55$ , together with their PDFs. (d) PDFs and time traces from the model with combined resistive and reactive asymmetries.

plotted in Fig. 2(a) for four  $\Phi$ . When  $\Phi = 0.5$ , the thermoacoustic system is linearly stable. The system's strongest resonance corresponds to an eigenmode whose azimuthal distribution exhibits one acoustic wavelength along the annular chamber circumference, and whose frequency is about 1090 Hz. The resonance oscillation of the different modes is sustained by the inherent broadband acoustic forcing from the turbulent combustion process. For larger  $\Phi$ , the acoustic energy production resulting from the constructive thermoacoustic feedback exceeds the acoustic energy dissipation, and the dominant eigenmode becomes linearly unstable. Under these conditions, thermoacoustic limit cycles are reached at the aforementioned resonance frequency, e.g. [42]. Their dynamics are governed by the nonlinear coherent response of the flame to the acoustic field and by the turbulent fluctuations of the heat release rate. Figure 2(b) presents the acoustic pressure  $p$  at three azimuthal locations during two short intervals (I) and (II) of the 100 s record for  $\Phi = 0.55$ , for which the self-sustained azimuthal thermoacoustic mode spins in the counterclockwise (CCW) and in the clockwise (CW) direction. Recently, a new ansatz for the acoustic pressure field based on quaternions was proposed to describe azimuthal eigenmodes in annular combustors [39]. A set of four state variables  $A, \theta, \chi$  and  $\varphi$ , which vary slowly with respect to the fast acoustic time scale  $2\pi/\omega$ , and which can be extracted from the acoustic pressure time series, allows the following well-defined description of the state of an azimuthal thermoacoustic mode

$$\tilde{p}(\Theta, t) = A(t) e^{i(\theta(t) - \Theta)} e^{-k\chi(t)} e^{j(\omega t + \varphi(t))}, \quad (1)$$

where  $t$  and  $\Theta$  are the time and the azimuthal coordinate, and  $i, j$  and  $k$  are the quaternion units. The acoustic pressure is  $\text{Re}(\tilde{p})$ , and  $A$  is the real-valued positive slowly-varying amplitude. The slowly varying angle  $\theta$  describes the position of the anti-nodal line [43]. The slowly varying angle  $\chi$  indicates whether the azimuthal eigenmode is a standing wave ( $\chi = 0$ ), a pure CW or CCW spinning wave ( $\chi = \mp\pi/4$ ) or a mix of both for  $0 < |\chi| < \pi/4$ . The angle  $\varphi$  stands for slow temporal

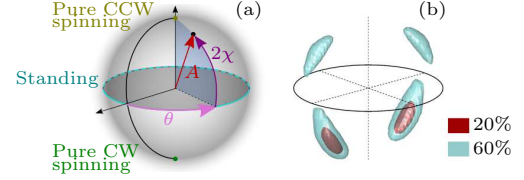


FIG. 3. (a) Bloch sphere representation of the state of the azimuthal mode. (b) Experimental joint PDF for  $\Phi = 0.55$ .

phase drift. These variables fully describe the acoustic fields  $p$  as a function of the time and azimuthal position. Figure 2(c) shows the time traces of the extracted slow-flow variables together with their probability density functions (PDFs) for the last 6 s of the record, an interval that is representative of the stationary dynamics when  $\Phi = 0.55$ . The joint PDF of the first three state variables deduced from the 100 s record at  $\Phi = 0.55$  is also shown in Fig. 3(b), where  $A, \theta$  and  $2\chi$  are taken as spherical coordinates as shown in Fig. 3(a). At the condition  $\Phi = 0.55$ , the amplitude of the azimuthal mode has a relatively small standard deviation compared to its mean value. The intermittent changes of sign of the nature angle  $\chi$  correspond to changes of spinning direction of the mixed mode, as shown in Fig. 2(b). Although the difference is small, the most probable orientation of the anti-nodal line of the mixed-mode's standing component is not the same whether the mode spins CW or CCW, a phenomenon that had never been reported and that will be explained later. We now consider the evolution of the state variable PDFs in the vicinity of the Hopf bifurcation. These stationary PDFs are shown in the left column of Fig. 4 for several  $\Phi$ . The evolution of  $P(A)$ , shown in Fig. 4(a), is typical of a supercritical Hopf bifurcation in presence of additive random forcing [44]. The bifurcation occurs around  $\Phi = 0.5125$ . This point separates broadband-noise-driven resonances, when the azimuthal thermoacoustic mode is linearly stable, from limit cycles, when it is linearly unstable. Next, one can consider how  $P(\varphi)$  changes with  $\Phi$  in Fig. 4(d). Overall, the slowly varying temporal phase  $\varphi$  drifts sufficiently during these

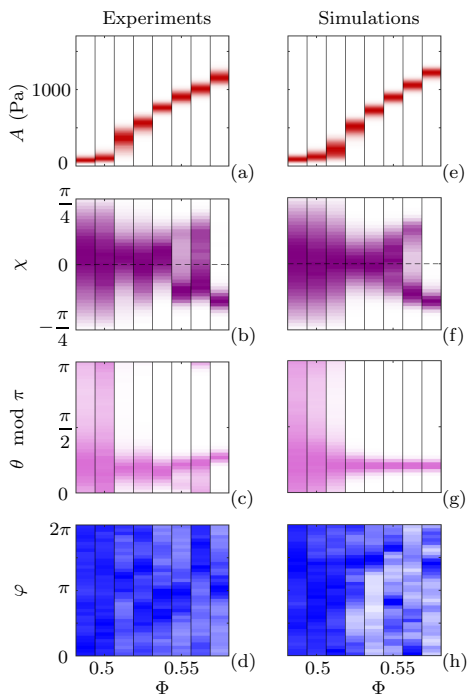


FIG. 4. Stationary PDFs of  $A$ ,  $\chi$ ,  $\theta$  and  $\varphi$  at several  $\Phi$  in the vicinity of the supercritical Hopf bifurcation. The PDFs are deduced from the slow-flow variable time traces, which are extracted from the acoustic pressure time traces following the procedure in [39]. For (a) to (d), the acoustic time traces were obtained experimentally. For (e) to (h), the acoustic time traces were obtained by simulating 100 s of Eq. (2). Linear dependencies with respect to  $\Phi$  of the parameters ( $\nu$ ,  $c_2\beta$ ,  $\kappa$ ,  $\Gamma$ ) were deduced from the data processing.

100 s records to yield rather flat distribution between 0 and  $2\pi$ . One can notice that some phases are statistically prevailing for the higher range of investigated  $\Phi$ , but these PDF maxima differ from case to case, and moreover, they wane when longer time traces are considered for computing the statistics, in agreement with the model which we propose in this letter. More interesting are the statistics of  $\theta$  and  $\chi$ . Let us begin with  $P(\theta)$  in Fig. 4(c): Even though the combustor was designed as rotationally symmetric as possible with a discrete rotational symmetry of order 12 (due to the 12 burners), the experimental results show a clearly preferred and repeatable anti-nodal line position for the different  $\Phi$ . Given the long run times and the high-order discrete rotational symmetry of the system, one would either expect a quasi-uniform distribution of  $\theta$  or a new preferred nodal line direction each time the combustor is ignited. The only explanation for this preferred orientation is the presence of a rotational symmetry breaking in the thermoacoustic system. Furthermore, in addition to this explicit symmetry breaking, the system exhibits a spontaneous symmetry breaking in terms of the nature of the thermoacoustic mode. When  $\Phi < 0.55$ ,  $P(\chi)$  is unimodal, with a maximum close to zero, indicating that the thermoacous-

tic mode is predominantly standing, which corroborates two recent theoretical studies [40, 45] that predicted the predominance of standing modes when the normalized stochastic forcing amplitude is large compared to the one of the limit cycle. For  $\Phi = 0.55$  and  $\Phi = 0.5625$ ,  $P(\chi)$  is bimodal: the spinning component of the mixed mode intermittently changes direction as illustrated in Fig. 2(c). Now, when  $\Phi = 0.575$  in Fig. 4(b), these sporadic reversals of spinning direction do not take place anymore: the mixed mode spins in the CW direction and the symmetry of its state PDF is spontaneously broken beyond this threshold. It is worth noting that other runs performed for  $\Phi \geq 0.575$ , can also lead to a robust CCW mixed mode. In the remainder of this letter, we present a model to explain the unexpected explicit symmetry breaking.

*Theoretical model and calibration of its parameters.*—In [40], the quaternion acoustic field was inserted into the following wave equation with distributed heat-release-rate fluctuations to model the thermoacoustic dynamics of an idealized thin annular chamber:

$$\frac{\partial^2 p}{\partial t^2} + \alpha \frac{\partial p}{\partial t} - \frac{c^2}{\mathcal{R}^2} \frac{\partial^2 p}{\partial \Theta^2} = (\gamma - 1) \frac{\partial \dot{Q}}{\partial t} + \Xi(\Theta, t). \quad (2)$$

In this equation,  $\alpha$  is the acoustic damping at the annulus boundaries,  $\mathcal{R}$  the annulus radius,  $c$  the speed of sound,  $\gamma$  the heat capacities ratio,  $\dot{Q}(\Theta, t)$  the *coherent* component of the heat release rate fluctuations and  $\Xi$  a spatially distributed white Gaussian noise representing the effect of *turbulent* fluctuations of the heat release rate [42, 46–48]. The coherent heat release rate fluctuations are then linked to the acoustic field using the expression  $(\gamma - 1)\dot{Q} = \beta [1 + c_2 \cos(2\Theta)]p - \kappa p^3$ . The first term stands for the linear response of the fluctuating heat release rate to acoustic perturbations. If  $\beta > \alpha$  and  $c_2 = 0$ , the linear growth rate of the thermoacoustic mode  $\nu = (\beta - \alpha)/2$  is positive, i.e. the mode is linearly unstable, and small acoustic perturbations are exponentially amplified. This pure exponential growth is not observed in real systems because of the inherent turbulence-induced stochastic forcing  $\Xi$  and because of the nonlinearity of the flame response to the acoustic field beyond a certain level. The first term also accounts for spatial non-uniformities along the annulus, through the second component  $c_2 \cos(2\Theta)$  of the Fourier expansion of any distribution of heat release rate source, which is the only component influencing the first azimuthal eigenmode [18]. The second term,  $-\kappa p^3$ , defines the saturation of flame response, which leads to limit cycle oscillations, and is sufficient to adequately capture the thermoacoustic dynamics in the vicinity of supercritical Hopf bifurcations [47, 49, 50], as in the present experiment. Further discussion about this heat release rate model is given in [41]. In [40], spatial and temporal averaging are performed to derive a system of coupled Langevin equations  $\dot{\mathbf{Y}} = \mathbf{F}(\mathbf{Y}) + \mathbf{B}(\mathbf{Y})\mathbf{N}$ , governing the dynamics of the

azimuthal mode state-vector  $\mathbf{Y} = (A, \chi, \theta, \varphi)^T$  via a deterministic contribution  $\mathbf{F}(\mathbf{Y})$  and a stochastic forcing term  $\mathbf{B}(\mathbf{Y})\mathbf{N}$ , where  $\mathbf{N} = (\zeta_A, \zeta_\chi, \zeta_\theta, \zeta_\varphi)^T$  is a vector of independent white Gaussian noises of intensity  $\Gamma/2\omega^2$ . The latter intensity involves the constant  $\Gamma$ , which is the spatially-averaged stochastic forcing level originating from the turbulent fluctuations of the heat release rate. The expressions for  $\mathbf{F}$  and  $\mathbf{B}$  are given in [40, 41] with the simplifying assumptions for their derivation. It is worth noting that this model cannot be used to predict the stability and slow-flow dynamics of a real combustor from the knowledge of its geometry and operating condition. However, we show here that its handful of parameters  $[\nu; c_2\beta; \kappa; \Gamma]$  can be identified from the experimental data and then the model can reproduce the thermoacoustic dynamics. Several methods are available for disentangling deterministic and stochastic contributions in stochastic trajectories, e.g. [51–53]. Here, we used the method developed in [54–57], which has already been taken up for investigating, among other areas, thermoacoustic and aeroacoustic problems, e.g. [49, 58]. First, for each  $\Phi$ , the transition probabilities of the state variables are extracted. Then, these probabilities are used to compute the first and second Kramers-Moyal coefficients that serve as basis for parameter identification with least square fitting. More details about the robustness of the parameter identification are given in [41]. It was found that simple linear regression for the dependencies of  $\nu$ ,  $c_2\beta$ ,  $\kappa$  and  $\Gamma$  upon  $\Phi$  allows to unravel the complex topology of the phase space. Indeed, time domain simulations of Eq. (2) were performed to generate 100s acoustic time series for each  $\Phi$ , from which the state variables and their statistics were extracted. The results are presented in Fig. 4(e) to 4(h), and are in close agreement with the experiments. This shows that despite the simplifications invoked to derive the low-order model, it can quantitatively reproduce the dynamics of the state variables.

*Discussion*—The two coupled equations for  $A$  and  $\chi$  recently allowed us to identify the fundamental mechanisms involved in the spontaneous symmetry breaking of the thermoacoustic mode state. In fact, the symmetry of the phase space is not broken, but beyond a certain linear growth rate, the symmetry of the state may be, if the mode chooses either the CW or the CCW spinning state and the noise is not sufficiently large to allow sporadic escape from and return to this attractor [59]. Here, we go significantly further by considering the stationary solutions of the Fokker-Planck equation governing the joint PDF of the state vector in order to provide a complete picture of the phase space topology (numerical method in [41]). We consider the reference case  $\Phi = 0.55$ , from which we arbitrarily change the linear growth rate  $\nu$  and the level of asymmetry  $c_2$  for fixed  $\kappa$  and  $\Gamma$ . These stationary solutions are presented in Fig. 5. We start in the bottom right corner, where the state exhibits a *unimodal* PDF corresponding to a statistically prevailing standing

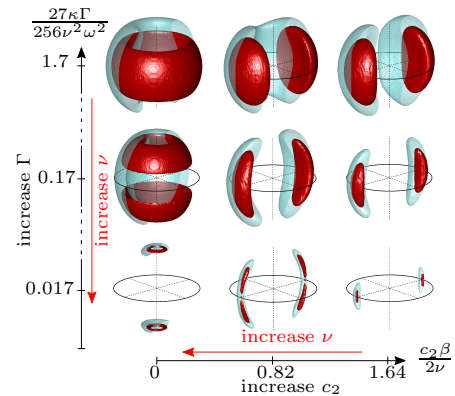


FIG. 5. Stationary PDF of the eigenmode state computed with the Fokker-Planck equation for different noise intensity  $\Gamma$  and asymmetry levels  $c_2$  (state probability: 20% and 60%). The reference case in the center of the bottom row corresponds to the parameters of the calibrated model for  $\Phi = 0.55$ .

mode with fixed anti-nodal line orientation [43]. When the rotational asymmetry level is decreased, the PDF first becomes *bimodal*, which corresponds to a predominant mixed mode with intermittent changes of spinning direction. Ultimately, for  $c_2 = 0$ , the nodal line cannot lock anymore on a fixed orientation, it slowly drifts as a random walk and the PDF takes the form of *two tori* close to the poles. These results are in line with previous findings from [18], which gave an incomplete description of the phase space topology. Then, the effect of noise and of the linear growth rate can be analyzed by moving vertically in the diagram. For an ideal rotationally symmetric combustor (first column) and for a fixed turbulent forcing level  $\Gamma$  and saturation constant  $\kappa$ , the effect of decreasing the linear growth rate is seen by moving up: the *two tori* merge when the system is brought close enough to the Hopf point (top row), which means that the system undergoes a transition from predominantly spinning states to prevailing standing modes with *single torus* PDF. However, a key consequence of the model, which had not been drawn so far, is that this toroidal PDF will not be observed in real combustors, because the more the source term gain  $\beta$  tends to  $\alpha$ , and thus  $\nu = (\beta - \alpha)/2 \rightarrow 0$ , the more  $c_2\beta/(\beta - \alpha)$  will rise, which means that such decrease of  $\beta$  would be accompanied with a move towards the right on the diagram. In other words, the effect of a *resistive* asymmetry, however minute, will be magnified in the vicinity of the bifurcation. Furthermore, we can add to the model tiny *reactive* asymmetries [60]. They also exist in real systems due to inherent geometrical imperfections, and cause, as shown in Fig. 2(d), the small changes of  $\theta$  synchronized with changes of spinning direction and the predominance of CW spinning modes for  $\Phi = 0.55$ . The spatial phase drift induced by these tiny imperfections is negligible during a few acoustic periods, but becomes significant over sufficiently long time scales. We can thus conclude that

manufacturing annular systems free from explicit symmetry breaking at the bifurcation is out of reach. Possible direct applications of this framework include the analysis of non-radial stellar pulsations [61–63], or the quest for weakly-dissipative nonreciprocal devices based on an acoustic analog of the Zeeman effect [7, 64], for which decreasing losses in circulators bring them closer to Hopf points where we show that slight asymmetries have considerable impact on wave dynamics.

This project has received funding from the European Union’s Horizon 2020 program (Grant 765998).

---

\* thomas.indlekofer@ntnu.no

† noirayn@ethz.ch

- [1] M. Kolář, T. Opatrný, and K.K. Das, “Criticality and spin squeezing in the rotational dynamics of a bose-einstein condensate on a ring lattice,” *Phys. Rev. A* **92** (2015).
- [2] G.E. Marti, R. Olf, and D.M. Stamper-Kurn, “Collective excitation interferometry with a toroidal bose-einstein condensate,” *Phys. Rev. A* **91** (2015).
- [3] Z. Shen, Y.-L. Zhang, Y. Chen, C.-L. Zou, Y.-F. Xiao, X.-B. Zou, F.-W. Sun, G.-C. Guo, and C.-H. Dong, “Experimental realization of optomechanically induced nonreciprocity,” *Nat. Photonics* **10**, 657–661 (2016).
- [4] J.-B. Ceppe, P. Féron, M. Mortier, and Y. Dumeige, “Dynamical analysis of modal coupling in rare-earth whispering-gallery-mode microlasers,” *Phys. Rev. Appl.* **11** (2019).
- [5] M. T. M. Woodley, L. Hill, L. Del Bino, G.-L. Oppo and P. Del’Haye, “Self-Switching Kerr Oscillations of Counterpropagating Light in Microresonators,” *Phys. Rev. Lett.* **126**, 043901 (2021).
- [6] B. Megyeri, G. Harvie, A. Lampis, and J. Goldwin, “Directional bistability and nonreciprocal lasing with cold atoms in a ring cavity,” *Phys. Rev. Lett.* **121**, 163603 (2018).
- [7] R. Fleury, D.L. Sounas, C.F. Sieck, M.R. Haberman, and A. Alù, “Sound isolation and giant linear nonreciprocity in a compact acoustic circulator,” *Science* **343**, 516–519 (2014).
- [8] J.E. Rice, I. Cziegler, P.H. Diamond, B.P. Duval, Y.A. Podpaly, M.L. Reinke, P.C. Ennever, M.J. Greenwald, J.W. Hughes, Y. Ma, E.S. Marmor, M. Porkolab, N. Tsujii, and S.M. Wolfe, “Rotation reversal bifurcation and energy confinement saturation in tokamak ohmic l-mode plasmas,” *Phys. Rev. Lett.* **107**, 265001 (2011).
- [9] F. Pétrélis, S. Fauve, E. Dormy, and J. P. Valet, “Simple mechanism for reversals of earth’s magnetic field,” *Phys. Rev. Lett.* **102**, 144503 (2009).
- [10] A. Sheyko, C.C. Finlay, and A. Jackson, “Magnetic reversals from planetary dynamo waves,” *Nature* **539**, 551–554 (2016).
- [11] J. D. Crawford and E. Knobloch, “Symmetry and symmetry-breaking bifurcations in fluid dynamics,” *Annu. Rev. Fluid Mech.* **23**, 341–387 (1991).
- [12] A. de la Torre and J. Burguete, “Slow dynamics in a turbulent von kármán swirling flow,” *Phys. Rev. Lett.* **99**, 054101 (2007).
- [13] Miguel López-Caballero and Javier Burguete, “Inverse cascades sustained by the transfer rate of angular momentum in a 3d turbulent flow,” *Phys. Rev. Lett.* **110**, 124501 (2013).
- [14] D. Faranda, Y. Sato, B. Saint-Michel, C. Wiertel, V. Padilla, B. Dubrulle and F. Daviaud, “Stochastic chaos in a turbulent swirling flow,” *Phys. Rev. Lett.* **119**, 014502 (2017).
- [15] Rayleigh, “The explanation of certain acoustical phenomena,” *Nature* **18**, 319–321 (1878).
- [16] W. Krebs, P. Flohr, B. Prade, and S. Hoffmann, “Thermoacoustic stability chart for high intensity gas turbine combustion system,” *Combust. Sci. Technol.* **174**, 99–128 (2002).
- [17] J. R. Seume, N. Vortmeyer, W. Krause, J. Hermann, C.-C. Hantschk, P. Zangl, S. Gleis, D. Vortmeyer, and A. Orthmann, “Application of active combustion instability control to a heavy duty gas turbine,” *J. Eng. Gas Turb. Power* **120**, 721–726 (1998).
- [18] N. Noiray and B. Schuermans, “On the dynamic nature of azimuthal thermoacoustic modes in annular gas turbine combustion chambers,” *Proc. R. Soc. London A* **469**, 20120535 (2012).
- [19] N. Worth and J.R. Dawson, “Modal dynamics of self-excited azimuthal instabilities in an annular combustion chamber,” *Combust. Flame* **160**, 2476–2489 (2013).
- [20] N. Worth and J.R. Dawson, “Effect of equivalence ratio on the modal dynamics of azimuthal combustion instabilities,” *Proc. Combust. Inst.* **36**, 3743–3751 (2017).
- [21] J. F. Bourgouin, D. Durox, J.P. Moeck, T. Schuller, and S. Candel, “Characterization and modeling of a spinning thermoacoustic instability in an annular combustor equipped with multiple matrix injectors,” *J. Eng. Gas Turb. Power* **137**, 021503 (2015).
- [22] P. Wolf, G. Staffelbach, L.Y.M. Gicquel, J-D. Mueller, and T. Poinsot, “Acoustic and large eddy simulation studies of azimuthal modes in annular combustion chambers,” *Combust. Flame* **159**, 3398–3413 (2012).
- [23] M. Bauerheim, F. Nicoud, and T. Poinsot, “Progress in analytical methods to predict and control azimuthal combustion instability modes in annular chambers,” *Phys. Fluids* **28**, 021303 (2016).
- [24] N.A. Worth and J.R. Dawson, “Self-excited circumferential instabilities in a model annular gas turbine combustor: Global flame dynamics,” *Proc. Combust. Inst.* **34**, 3127–3134 (2013).
- [25] M. Bauerheim, P. Salas, F. Nicoud, and T. Poinsot, “Symmetry breaking of azimuthal thermo-acoustic modes in annular cavities: A theoretical study,” *J. Fluid Mech.* **760**, 431–465 (2014).
- [26] J. F. Bourgouin, D. Durox, J.P. Moeck, T. Schuller, and S. Candel, “A new pattern of instability observed in an annular combustor: The slanted mode,” *Proc. Combust. Inst.* **35**, 3237–3244 (2015).
- [27] F.M. Berger, T. Hummel, B. Schuermans, and T. Sattelmayer, “Pulsation-amplitude-dependent flame dynamics of high-frequency thermoacoustic oscillations in lean-premixed gas turbine combustors,” *Journal of Engineering for Gas Turbines and Power* **140**, 041507 (2018).
- [28] J.-W. Kim, W. Gillman, B. Emerson, D. Wu, T. John, V. Acharya, M. Isono, T. Saitoh and T. Lieuwen, “Modal dynamics of high-frequency transverse combustion instabilities,” *Proc. Combust. Inst.* **38** (2021).
- [29] S. Evesque, W. Polifke, and C. Pankiewicz, “Spin-

- ning and azimuthally standing acoustic modes in annular combustors,” AIAA/CEAS Aeroacoustics Conf. **9**, 3182 (2003).
- [30] B. Schuermans, C.O. Paschereit, and P. Monkewitz, “Non linear combustion instabilities in annular gas turbine combustors,” AIAA Aerospace Sciences Meeting and Exhibit **44**, 0549 (2006).
- [31] N. Noiray, M. Bothien, and B. Schuermans, “Analytical and numerical analysis of staging concepts in annular gas turbines,” *Combust. Theor. Model.* **15**, 585–606 (2011).
- [32] G. Ghirardo, M.P. Juniper, and J.P. Moeck, “Weakly nonlinear analysis of thermoacoustic instabilities in annular combustors,” *J. Fluid Mech.* **805**, 52–87 (2016).
- [33] L. Magri, M. Bauerheim, F. Nicoud, and M.P. Juniper, “Stability analysis of thermo-acoustic nonlinear eigenproblems in annular combustors. part ii. uncertainty quantification,” *J. Comput. Phys.* **325**, 411–421 (2016).
- [34] T. Hummel, F. Berger, N. Stadlmair, B. Schuermans, and T. Sattelmayer, “Extraction of linear growth and damping rates of high-frequency thermoacoustic oscillations from time domain data,” *J. Eng. Gas Turb. Power* **140**, 051505 (2018).
- [35] J. P. Moeck, D. Durox, T. Schuller, and S. Candel, “Nonlinear thermoacoustic mode synchronization in annular combustors,” *Proc. Combust. Inst.* **37**, 5343–5350 (2018).
- [36] A. Orchini, G.A. Mensah, and J.P. Moeck, “Effects of nonlinear modal interactions on the thermoacoustic stability of annular combustors,” *J. Eng. Gas Turb. Power* **141** (2019).
- [37] D. Yang, D. Laera, and A.S. Morgans, “A systematic study of nonlinear coupling of thermoacoustic modes in annular combustors,” *J. Sound Vib.* **456**, 137–161 (2019).
- [38] P.E. Buschmann, G.A. Mensah, and J.P. Moeck, “Intrinsic thermoacoustic modes in an annular combustion chamber,” *Combust. Flame* **214**, 251–262 (2020).
- [39] G. Ghirardo and M.R. Bothien, “Quaternion structure of azimuthal instabilities,” *Phys. Rev. Fluids* **3**, 113202 (2018).
- [40] A. Faure-Beaulieu and N. Noiray, “Symmetry breaking of azimuthal waves: Slow-flow dynamics on the bloch sphere,” *Phys. Rev. Fluids* **5**, 023201 (2020).
- [41] “See supplemental material.”
- [42] N. Noiray and B. Schuermans, “Deterministic quantities characterizing noise driven hopf bifurcations in gas turbine combustors,” *Int. J. Nonlin. Mech.* **50**, 152–163 (2012).
- [43] “The eigenmode state is identical for  $\theta$  and  $\theta + \pi$ .”
- [44] A. Juel, A. G. Darbyshire, and T. Mullin, “The effect of noise on pitchfork and hopf bifurcations,” *Proc. R. Soc. A* **453**, 2627–2647 (1997).
- [45] G. Ghirardo and F. Gant, “Averaging of thermoacoustic azimuthal instabilities,” *J. Sound Vib.* **490**, 115732 (2021).
- [46] P. Clavin, J.S. Kim, and F.A. Williams, “Turbulence-induced noise effects on high-frequency combustion instabilities,” *Combust. Sci. Technol.* **96**, 61–84 (1994).
- [47] T.C. Lieuwen, “Statistical characteristics of pressure oscillations in a premixed combustor,” *J. Sound Vib.* **260**, 3–17 (2003).
- [48] T. Lieuwen and A. Banaszuk, “Background noise effects on combustor stability,” *J. Propul. Power* **21**, 25–31 (2005).
- [49] N. Noiray and A. Denisov, “A method to identify thermoacoustic growth rates in combustion chambers from dynamic pressure time series,” *Proc. Combust. Inst.* **36**, 3843–3850 (2017).
- [50] M. Lee, K. T. Kim, V. Gupta, and L. K. B. Li, “System identification and early warning detection of thermoacoustic oscillations in a turbulent combustor using its noise-induced dynamics,” *Proc. Combust. Inst.* **38** (2021).
- [51] A. Frishman and P. Ronceray, “Learning force fields from stochastic trajectories,” *Phys. Rev. X* **10**, 021009 (2020).
- [52] F. Ferretti, V. Chardès, T. Mora, A. M. Walczak, and I. Giardina, “Building general langevin models from discrete datasets,” *Phys. Rev. X* **10**, 031018 (2020).
- [53] D. B. Brückner, P. Ronceray, and C. P. Broedersz, “Inferring the dynamics of underdamped stochastic systems,” *Phys. Rev. Lett.* **125**, 058103 (2020).
- [54] S. Siegert, R. Friedrich, and J. Peinke, “Analysis of data sets of stochastic systems,” *Phys. Lett. A* **243**, 275–280 (1998).
- [55] R. Friedrich, Ch. Renner, M. Siefert, and J. Peinke, “Comment on “Indispensable Finite Time Corrections for Fokker-Planck Equations from Time Series Data”,” *Phys. Rev. Lett.* **89**, 149401 (2002).
- [56] F. Böttcher, J. Peinke, D. Kleinhans, R. Friedrich, P. G. Lind, and M. Haases, “Reconstruction of Complex Dynamical Systems Affected by Strong Measurement Noise,” *Phys. Rev. Lett.* **97**, 090603 (2006).
- [57] R. Friedrich, J. Peinke, M. Sahimi, and M. Reza Rahimi Tabar, “Approaching complexity by stochastic methods: From biological systems to turbulence,” *Phys. Rep.* **506**, 87–162 (2011).
- [58] E. Boujo, C. Bourquard, Y. Xiong, and N. Noiray, “Processing time-series of randomly forced self-oscillators: The example of beer bottle whistling,” *J. Sound Vib.* **464**, 114981 (2020).
- [59] A. Faure-Beaulieu, T. Indlekofer, J. Dawson, and N. Noiray, “Experiments and low-order modelling of intermittent transitions between clockwise and anticlockwise spinning thermoacoustic modes in annular combustors,” *Proc. Combust. Inst.* **38** (2021).
- [60] “In the model which combines resistive and reactive asymmetries, the last term of the l.h.s. of eq. (2) is multiplied by  $[1 + \varepsilon \cos(2[\theta - \vartheta])]$ . fixing  $\nu$ ,  $\kappa$  and  $\gamma$  to their values from fig. 4, the calibration for  $\phi = 0.55$  of this model variant yields  $\varepsilon = 0.0023$  and  $\vartheta = 0.03$  and  $c_2\beta = 17 \text{ s}^{-1}$ .”
- [61] J. R. Buchler, M.-J. Goupil, and T. Serre, “Dynamic pulsation amplitudes for a rotationally split nonradial mode - the  $l = 1$  case,” *Astron. Astrophys.* **296**, 405–417 (1995).
- [62] J. R. Buchler, M.-J. Goupil, and G. Kovács, “Stellar pulsations with stochastic driving,” *Astron. Astrophys.* **280**, 157–168 (1993).
- [63] C. Aerts, “Probing the interior physics of stars through asteroseismology,” *Rev. Modern Phys.* **93**, 015001 (2021).
- [64] Y. Ding, Y. Peng, Y. Zhu, X. Fan, J. Yang, B. Liang, X. Zhu, X. Wan, and J. Cheng, “Experimental demonstration of acoustic chern insulators,” *Phys. Rev. Lett.* **122**, 014302 (2019).